Phosphorylation of Rat Aquaporin-4 at Ser^{111} Is Not Required for Channel Gating

Mette Assentoft,[1] Shreyas Kaptan,[2] Robert A. Fenton,[3] Susan Z. Hua,[4,5] Bert L. de Groot,[2] and Nanna MacAulay[1]

Aquaporin 4 (AQP4) is the predominant water channel in the mammalian brain and is mainly expressed in the perivascular glial endfeet at the brain-blood interface. AQP4 has been described as an important entry and exit site for water during formation of brain edema and regulation of AQP4 is therefore of therapeutic interest. Phosphorylation of some aquaporins has been proposed to regulate their water permeability via gating of the channel itself. Protein kinase (PK)-dependent phosphorylation of Ser^{111} has been reported to increase the water permeability of AQP4 expressed in an astrocytic cell line. This possibility was, however, questioned based on the crystal structure of the human AQP4. Our study aimed to resolve if Ser^{111} was indeed a site involved in phosphorylation-mediated gating of AQP4. The water permeability of AQP4-expressing *Xenopus* oocytes was not altered by a range of activators and inhibitors of PKG and PKA. Mutation of Ser^{111} to alanine or aspartate (to prevent or mimic phosphorylation) did not change the water permeability of AQP4. PKG activation had no effect on the water permeability of AQP4 in primary cultures of rat astrocytes. Molecular dynamics simulations of a phosphorylation of AQP4.Ser^{111} recorded no phosphorylation-induced change in water permeability. A phospho-specific antibody, exclusively recognizing AQP4 when phosphorylated on Ser^{111}, failed to detect phosphorylation in cell lysate of rat brain stimulated by conditions proposed to induce phosphorylation of this residue. Thus, our data indicate a lack of phosphorylation of Ser^{111} and of phosphorylation-dependent gating of AQP4.

GLIA 2013;61:1101–1112

Key words: regulation; astrocytic swelling; AQP4; protein kinase G; molecular dynamics simulations

Introduction

Aquaporins possess intrinsic water permeability when faced with an osmotic gradient and a subset of the 13 isoforms identified in humans displays additional permeability toward glycerol, urea, and ammonium (reviewed by Gomes et al. (2009)). AQP4 is the predominant aquaporin in the mammalian brain and is localized in the perivascular glial endfeet, the ependymal cell lining, and osmosensing areas such as the supraoptic nucleus and subfornical organ (Nielsen et al., 1997). AQP4 exists as three functional isoforms with different length of their N-termini and distinct isoform-specific water permeability (Fenton et al., 2010; Moe et al., 2008). The shortest isoform (M23) is the dominant AQP4 isoform in the brain (Moe et al., 2008).

AQP4 has been proposed to be involved in brain edema formation based on its distinct expression pattern at the brain-blood interface and the altered outcome of AQP4 knock-out mice following experimentally inflicted brain edema formation (reviewed by Zador et al. (2009)). Short-term regulation of AQP4 under pathophysiological conditions promoting brain edema has therefore attracted scientific interest. Dynamic regulation of AQP4 could be achieved by changes in levels of AQP4 membrane expression or by changes in the water permeability of AQP4 already present in

View this article online at wileyonlinelibrary.com. DOI: 10.1002/glia.22498

Published online Apr 25, 2013 in Wiley Online Library (wileyonlinelibrary.com). Received Sep 6, 2012, Accepted for publication Feb 27, 2013.

Address correspondence to Nanna MacAulay, Department of Cellular and Molecular Medicine, University of Copenhagen, Blegdamsvej 3, Bldg. 12.6, 2200 Copenhagen N, Denmark. E-mail: macaulay@sund.ku.dk

From the [1]Department of Cellular and Molecular Medicine, University of Copenhagen, Copenhagen, Denmark; [2]Computational Biomolecular Dynamics Group, Max Planck Institute for Biophysical Chemistry, Gottingen, Germany; [3]Department of Biomedicine and InterPrET Center, Aarhus University, Aarhus, Denmark; [4]Department of Physiology and Biophysics, State University of New York in Buffalo, Buffalo, NY; [5]Department of Mechanical and Aerospace Engineering, State University of New York in Buffalo, Buffalo, NY.

the membrane, i.e., "gating." The possibility of altered membrane expression of AQP4 following experimentally inflicted brain edema has remained inconclusive based on divergent reports of up-regulation (Papadopoulos and Verkman 2005; Ribeiro Mde et al., 2006; Saadoun et al., 2003) and down-regulation (Friedman et al., 2009; Frydenlund et al., 2006; Meng et al., 2004; Zhao et al., 2005) of AQP4 expression during edema formation. Activation of PKC leads to down-regulation of AQP4 function (Zelenina et al., 2002) possibly by internalization of the protein (Moeller et al., 2009a). Other protein kinases such as PKG and PKA have been proposed to phosphorylate Ser^{111} in AQP4 and thereby provoke a gating event leading to increased osmotic water permeability (Gunnarson et al., 2008; Song and Gunnarson, 2012). Phosphorylation-dependent gating of aquaporins has been promoted further following molecular dynamics simulations performed on the crystallized spinach aquaporin, SoPIP2;1. In the study, the authors added, *in silico,* a phosphate-moiety to the Ser^{115} (Tornroth-Horsefield et al., 2006), which corresponds to Ser^{111} in AQP4. The molecular dynamics recorded an open conformation of SoPIP2;1 upon this phosphorylation.

Despite the beauty of this gating model, concerns have been raised: Crystallization of the human AQP4 yielded an open conformation, despite the lack of a phosphate group at Ser^{111}, and a D-loop too short to act as the gate (Ho et al., 2009). *In vivo* phosphorylation of Ser^{115} on SoPIP2;1 was not detected despite experimental activation of a range of protein kinases (Johansson et al., 1998). In addition, the open structure of the spinach aquaporin, on which the molecular modeling was based, was obtained at a pH promoting a closed structure and vice versa (Tornroth-Horsefield et al., 2006; Walz et al., 2009). In this study we aimed to determine the extent to which AQP4 is gated by phosphorylation of Ser^{111}. We found no evidence in favor of phosphorylation-dependent gating of AQP4 in its native setting in primary culture of astrocytes, upon heterologous expression in *Xenopus* oocytes, or by molecular dynamics simulations. Nor did we detect *in vivo* phosphorylation of the Ser^{111} in rat brain.

Materials and Methods

Molecular Biology

Rat AQP4.M23, human KCNQ1, KCNE1, and ENaC were subcloned into the oocyte expression vector pXOOM (AQP4.M23, KCNQ1, and KCNE1) or pBS (ENaC), linearized downstream from the poly-A segment, and *in vitro* transcribed using T7 mMessage Machine (Ambion, Austin, TX). cRNA was extracted with MEGAclear (Ambion, Austin, TX) and micro-injected into defolliculated *Xenopus laevis* oocytes (25 ng AQP4 or ENaC (1:1:1 of the α, β, and γ subunit) RNA/oocyte or 5 ng KCNQ1/KCNE1 (4:1) RNA/oocyte). Mutations were introduced into AQP4 with Quick Change site-directed mutagenesis kit (Stratagene, Santa Clara, CA) and verified with DNA sequencing. Numbering of the AQP4 amino acids is kept according to that of AQP4.M1.

Oocyte Preparation

Xenopus laevis frogs were obtained from Nasco (Fort Atkinson, WI) or National Center for Scientific Research (France). Oocytes were surgically removed from anesthetized frogs and prepared as previously described (Fenton et al., 2010). The protocol complies with the European Community guidelines for the use of experimental animals and the experiments were approved by The Danish National Committee for Animal Studies.

Oocyte Volume Measurements

The experimental setup for measuring water permeability of oocytes has been described in detail previously (Zeuthen et al., 2006). Briefly, the oocyte was placed in a small chamber with a glass bottom and perfused with a control solution (100 mM NaCl, 2 mM KCl, 1 mM $CaCl_2$, 1 mM $MgCl_2$, 10 mM HEPES, pH 7.4) at room temperature. Oocyte images were captured continuously from below at a rate of 25 images/s. To determine the water permeability, the oocytes were challenged with a hypertonic solution (control solution with additional 20 mOsm mannitol).

Immunocytochemistry and Confocal Laser Scanning Microscopy

Fixed oocytes were prepared for immunocytochemistry as previously described (Moeller et al., 2009b) and the 2 μm sections were immunostained with an anti-AQP4 antibody 1:5,000 (Alomone Laboratories, Israel) while an Alexa 488-conjugated secondary antibody 1:1,000 was used for visualization (DAR, Invitrogen, Denmark). Imaging, image semi-quantification, and validation was performed as recently described in detail (Moeller et al., 2009b).

Electrophysiology

Conventional two-electrode voltage clamp studies were performed with a DAGAN CA-1B High Performance oocyte clamp (DAGAN, Minneapolis, MN) with DigiData 1322A interface controlled by pCLAMP software, version 9.2 (Axon Instruments, Burlingame, CA). For ENaC measurements the membrane potential was clamped at -50 mV and the current–voltage (I–V) relationship was determined by stepping the clamp potential from -50 mV to test potentials ranging from $+40$ mV to -120 mV in 20 mV increments (100 ms pulses). For KCNQ1/KCNE1 measurements, the membrane potential was clamped at -80 mV. The I–V relationship was obtained with a 2 s pulse to a range of voltages between -80 mV and $+60$ mV in 20 mV steps followed by a 1 s pulse to -40 mV.

Astrocyte Preparation

Adult male Sprague-Dawley rats (250–300 g) were used for the astrocytic preparation. The procedure has earlier been described in detail (Langan et al., 1995) and these cultured astrocytes have previously been used for volume measurements (see below and Ateya et al. (2005)). In brief, adult astrocytes were isolated from gelatin-sponge implants left in the animal for three days. Sponges were subsequently removed, minced and triturated followed by trypsination

and passage through a nylon mesh with pore diameter of 20 μm. The astrocytes were maintained in Dulbecco's Modified Eagle Medium (DMEM) supplemented with 10% fetal bovine serum and 1% penicillin/streptomycin. Cells were used in experiments two to five days after passage. Cells between passage 5 and 15 were used and expression of AQP4 verified with Western blotting (data not shown).

Astrocyte Volume Measurements

A microfluidic volume sensor was used to study volume changes in astrocytes, as previously described (Ateya et al., 2005). Astrocytes were grown on a microscope slide that was inverted over the sensor chip thereby creating a flow chamber with a fixed volume of 60 nL. A sinusoidal current of 50 Hz, 1 μA was provided to the two outer electrodes in the chamber and the voltage was measured between the two inner electrodes. An increase in cell volume will increase the chamber resistance and thus an increase in voltage serves as the functional read-out of cell swelling. The chamber was perfused with an isotonic solution (95 mM NaCl, 5 mM KCl, 1.2 mM $CaCl_2$, 1 mM $MgCl_2$, 5 mM HEPES, 20 mM glucose, 100 mM mannitol, pH 7.4), 310 mOsm at room temperature. The flow rate of the solution ($\sim$30 μL/min) was controlled by adjusting hydraulic pressure at the inlet. To study the water permeability, the astrocytes were challenged with a hypotonic solution (isotonic solution with 60 mM less mannitol), 250 mOsm.

Molecular Dynamics Simulations

The starting structure of AQP4 was obtained from the protein data bank, entry 3GD8 (Ho et al., 2009). The protein was embedded in a membrane bilayer made up of 294 dimyristoylphosphotidylcholine (DMPC) lipids, using the Gromacs tool g_membed (Wolf et al., 2010). An ion concentration of 150 mM NaCl was chosen to simulate a neutral system. All the simulations were performed using the Gromacs simulation package version 4.5 (Hess et al., 2008). The AMBER99SB-ILDN force field was used for the protein and the ions (Lindorff-Larsen et al., 2010) and the parameters for the lipids were derived from Berger et al. (1997). The box was hydrated with 22,010 molecules of SPC water (Berendsen et al., 1987). The electrostatics in the system were treated explicitly within a cut-off of 1.0 nm and with the Particle Mesh Ewald method for the rest of the system (Darden et al., 1993). A cut-off of 1.0 nm was used for the calculation of Lennard-Jones interactions. The LINCS algorithm was used to constrain the bonds in the system (Hess 2008) along with v-sites for the protein hydrogens (Feenstra et al., 1999) allowing a time-step of 4 fs. The simulation temperature was held constant at 300 K using velocity-rescale thermostat (Bussi et al., 2007) with a coupling constant of 0.5 ps. The pressure was maintained at 1 atm with the Parrinello-Rahman barostat. AQP4 was simulated under two conditions: with no modifications to the amino acid sequence and with phosphorylation of Ser^{111}. The parameters for the phosphorylated serine residue were obtained from Homeyer et al. (2006). The simulations were carried out for 500 ns each and the water permeability was calculated using the collective diffusion method (Zhu et al., 2004). The first 100 ns of the simulations were discarded to account for equilibration. The osmotic water permeability was then calculated for a 50 ns window, dividing the simulation into eight slices for each monomer. The average over the eight windows and four monomers was used to compare the water permeability of AQP4 with its phosphorylated form.

Preparation of Rat Brain Lysate and Immunoblotting

Male Sprague–Dawley rats (3–4 weeks) were anesthetized and decapitated. The brains were immediately removed and placed in ice-cold artificial cerebrospinal fluid (aCSF) (125 mM NaCl, 2.5 mM KCl, 26 mM $NaHCO_3$, 1.25 mM NaH_2PO_4, 1 mM $MgCl_2$, 2 mM $CaCl_2$, 25 mM glucose, pH 7.4). The brains were cut into 0.5 mm thick slices and incubated in the presence or absence of the group I mGluR agonist (*S*)-3,5 dihydroxyphenylglycine (DHPG) (50 μM) for 60 min at 35°C in aCSF bubbled with 95% O_2 and 5% CO_2. The slices were homogenized on ice in cold homogenizing buffer (50 mM Tris pH 7.4, 2.5 mM Na-EGTA, 5 mM Na-EDTA, 10 mM NaCl, 10 mM KCl, 100 mM NaFl, 320 mM sucrose, 200 μg/mL pefabloc, 2 μg/mL aprotinin, 1 μg/mL leupeptin, 2 μg/mL antipain, 10 μg/mL benzamidine and PhosSTOP Phosphatase Inhibitor Cocktail 1 tablet per 10 mL), and cell debris was pelleted at 800*g*, 4°C x 10 min. The supernatant was subsequently centrifuged at 15,500*g*, 4°C $\times$ 90 min and pellet was resuspended in cold lysis buffer (50 M Tris pH 8.5, 150 mM NaCl, 5 mM EDTA, 1% Nonidet P40, 8 μM leupeptin, 0.4 mM pefablock, and PhosSTOP Phosphatase Inhibitor Cocktail, 1 tablet per 10 mL) and snap frozen. Immunoblotting was performed (10 μg protein/lane) with rabbit anti-AQP4 antibody, 1:1,000 (Alomone Laboratories, Jerusalem, Israel) or a custom-made rabbit anti-pS111-AQP4 antibody, 1:1,000 (PhosphoSolutions®, Aurora, CO). Two peptides (CTRKISIAK either phosphorylated at the serine residue (the epitope) or non-phosphorylated) were synthesized by Phosphosolutions® and are published with their permission (Aurora, CO). For dot blot, the peptides (20 ng) were spotted onto a membrane and probed with the custom-made rabbit anti-pS111-AQP4 antibody, 1:1,000. A horseradish peroxidase-conjugated secondary antibody (P448, Dako, Denmark) was used at 1:3,000. Visualization was obtained with SuperSignal West Pico Chemiluminescent Substrate (Thermo Fisher Scientific, Waltham, MA) and imaged with BioSpectrum AC imaging system (UVP, Upland, CA).

Drugs

Dihydroxyphenylglycine, DHPG (50 μM), 8-Br-cGMP (100 μM), 8-pCPT-cGMP (100 μM), H89 (50 μM), pefabloc (200 μg/mL), leupeptin (1 μg/mL), aprotinin (2 μg/mL), antipain (2 μg/mL), and benzamidine (10 μg/ml) were all dissolved in water. Amiloride (100 μM) and K252a (1 μM) were dissolved in DMSO (0.067% or 0.05% DMSO in both control and test solution) while 8-Br-cAMP (300 μM) was dissolved in water containing 100 mM TRIS-base. All were obtained from Sigma Aldrich, Denmark. PhosSTOP Phosphatase Inhibitor Cocktail Tablets (1 tablet per 10 mL) and Nonidet P40 (1%) were obtained from Roche, Germany.

Statistics

Data are presented as means $\pm$ SEM. Student's *t*-test or analysis of variance (ANOVA) followed by Dunnett's multiple comparison test

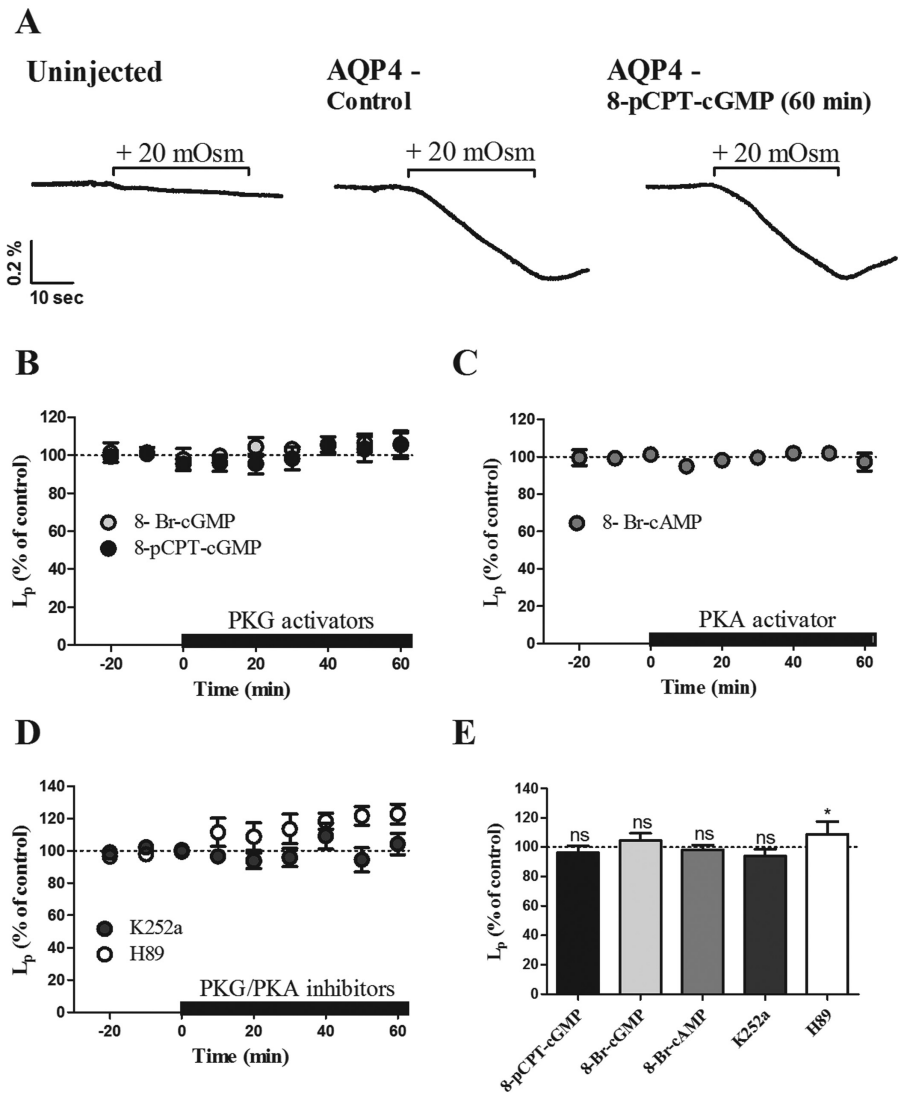

FIGURE 1: No PKG/PKA-dependent regulation of AQP4 expressed in oocytes. (A) Volume traces from an uninjected oocyte challenged with a hyperosmotic gradient (left panel) and an AQP4-expressing oocyte challenged with a hyperosmotic gradient before and after exposure to 100 μM 8-pCPT-cGMP for 60 min (middle and right panel). (B–D) The relative water permeability of AQP4-expressing oocytes determined as a function of time. Three control measurements were taken prior to addition of either (B) PKG activators (8-pCPT-cGMP, 100 μM or 8-Br-cGMP, 100 μM), (C) a PKA activator (8-Br-cAMP, 300 μM) or (D) PKG and PKA inhibitors (K252a, 1 μM or H89, 50 μM) to the external solution (black bar) (n = 7–12). (E) A summary of the water permeability of AQP4-expressing oocytes after 20 min exposure to various PKG and PKA activators and inhibitors relative to the control measurements. In % of control; 96.2 ± 4.6 for 8-pCPT-cGMP, n = 12, 104.4 ± 4.8 for 8-Br-cGMP, n = 7, 98.2 ± 3.3 for 8-Br-cAMP, n = 7, 93.9 ± 5.0 for K252a, n = 8, and 108.8 ± 8.5 for H89, n = 8. Repeated measures ANOVA followed by Dunnett's multiple comparison test was used as statistical test. *P < 0.05.

were used for the statistical analysis. A probability level of <0.05 was considered statistically significant.

Results

To determine the effect of a putative PKG-dependent phosphorylation of AQP4, the M23 isoform of AQP4 was heterologously expressed in *Xenopus laevis* oocytes. The osmotic water permeability of the oocytes was evaluated upon an abrupt challenge with a hypertonic test solution containing an additional 20 mM mannitol (20 mOsm). This osmotic challenge caused a ~15-fold faster shrinkage of AQP4-expressing oocytes compared to that of the native uninjected oocytes (compare $1.48 \pm 0.05 \times 10^{-3}$ cm/s ($n = 77$) with $0.09 \pm 0.01 \times 10^{-3}$ cm/s ($n = 34$), $P < 0.05$), representative traces shown in Fig. 1A, left and middle trace. This experimental system thus provides us with a clear read-out of AQP4 function with a negligible background due to the low inherent water permeability of the oocyte membrane. Following three water permeability measurements in control solution to ensure a stable baseline, PKG was activated by addition of membrane-permeable cGMP analogs (100 μM 8-Br-cGMP or 8-pCPT-cGMP) to the test solutions. The water permeability

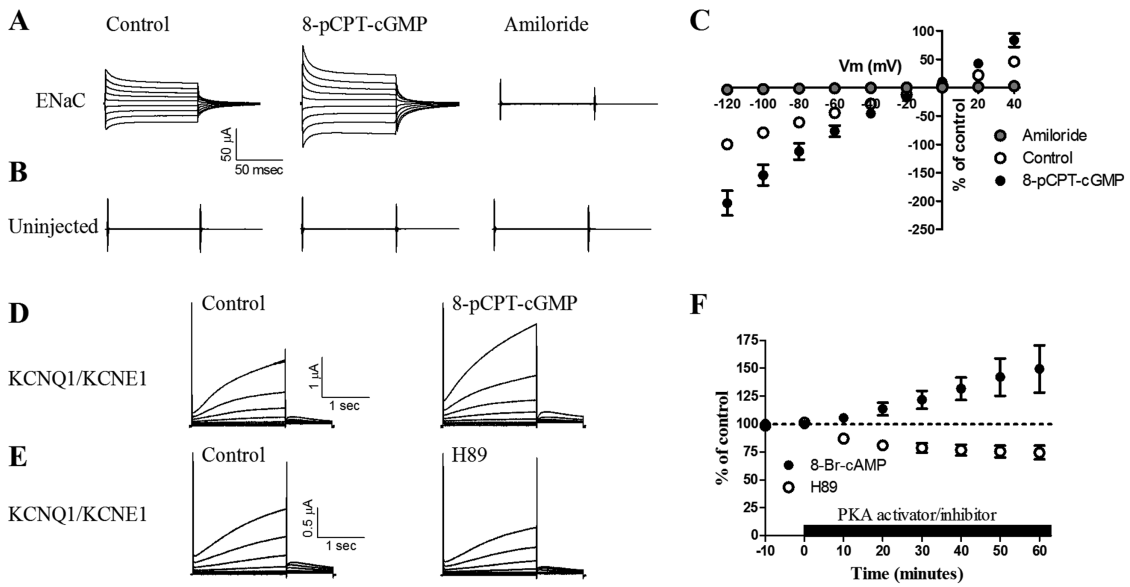

FIGURE 2: PKG/PKA activation in oocytes. (A, B) *I/V* relationship of an oocyte expressing ENaC (A) or an uninjected oocyte (B) before and after 5 min treatment with a PKG-activator (8-pCPT-cGMP, 100 μM), left and middle panel. The same oocyte was subsequently exposed to 100 μM of the ENaC blocker amiloride (right panel). (C) A summary of the *I/V* relationship of ENaC-expressing oocytes (n = 4) before and after treatment with 8-pCPT-cGMP and amiloride relative to the control measurement at −120 mV. In % of control at V_m = −120 mV: 203.5 ± 20.4 for 8-pCPT-cGMP ($P < 0.05$) and 3.8 ± 1.5 for amiloride ($P < 0.05$). (D, E) *I/V* relationship of oocytes expressing KCNQ1/KCNE1 before and after 60 min treatment with either a PKA-activator (8-Br-cAMP, 300 μM) (D) or PKA/PKG inhibitor (H89, 50 μM) (E). (F) Summary of the membrane currents obtained in KCNQ1/KCNE1-expressing oocytes after 60 min exposure to either 8-Br-cAMP (n = 5) or H89 (n = 3) relative to the control measurements. In % of control at V_m = 20 mV: 149.5 ± 21.3 for 8-Br-cAMP ($P < 0.05$) and 74.4 ± 6.1 for H89 ($P < 0.05$). Repeated measures ANOVA followed by Dunnett's multiple comparison test was used as statistical test.

was then measured in 10-min intervals for 60 min. The rate of shrinkage of the same AQP4-expressing oocyte following 60 min exposure to 8-pCPT-cGMP is illustrated in Fig. 1A, right trace. Figure 1B shows the water permeability as a function of time for AQP4-expressing oocytes, with the addition of 8-pCPT-cGMP or 8-Br-cGMP marked with a black bar. No significant change in AQP4-induced water permeability was observed upon activation of PKG (n = 12 and 7), data for 20 min PKG-activation are summarized in Fig. 1E. The amino acid sequence surrounding Ser^{111} encodes a consensus sequence for PKG as well as PKA. Thus the effect on AQP4 function by activation of PKA was determined by addition of a membrane-permeable cAMP analog (300 μM 8-Br-cAMP). The water permeability of AQP4-expressing oocytes was not altered upon this treatment, n = 8 (Fig. 1C), summarized for 20 min PKA activation in Fig. 1E. To rule out the possibility that the steady-state level of Ser^{111} phosphorylation in oocytes was too high to allow for further kinase-dependent activation, similar experiments were performed with membrane-permeable inhibitors of PKA and PKG; 50 μM H89 or 1 μM K252a (Johansson et al., 1998; Rusinova et al., 2009), n = 8 (Fig. 1D). K252a had no significant effect on the water permeability but kinase inhibition with H89 produced a slight increase in AQP4-mediated water permeability (n = 8, $P < 0.05$), which may be due to its inhibitory action on PKC, the activation of which leads to down-regulation of AQP4 (Moeller et al., 2009a). The intrinsic water permeability of batch-matched uninjected oocytes was not affected by any of the above treatments (data not shown). Thus, we observed no indication of kinase activation leading to the proposed increase in AQP4-mediated water permeability nor of kinase inhibition leading to reduction thereof.

With the lack of both PKG- and PKA-induced increase in AQP4-dependent water permeability, we verified the kinase activity in the oocytes by expressing either the epithelial Na^+ channel (ENaC) known to be activated by PKG (Nie et al., 2009) or the PKA-regulated voltage-gated potassium channel KCNQ1, with its ancillary subunit KCNE1 (Dilly et al., 2004; Grunnet et al., 2003). ENaC-expressing oocytes were voltage clamped and the *I–V* relation was determined (Fig. 2A, left trace). Subsequently, the same ENaC-expressing oocyte was exposed to 8-pCPT-cGMP (100 μM) for 5 min with a subsequent determination of the *I–V* relation (Fig. 2A, middle trace). PKG activation increased the ENaC-mediated current obtained at −120 mV to 203.5 ± 20.4% of control, n = 4 (Fig. 2C) but had no effect on the uninjected oocytes, 91.7 ± 3.3% of control, n = 3 (Fig. 2B). The ENaC blocker amiloride (100 μM) completely abolished the ENaC current (Fig. 2A, right trace and 2C). The *I–V* relation of KCNQ1/KCNE1-expressing oocytes was determined before

(Fig. 2D,E, left traces) and after exposure to the PKA activator 8-Br-cAMP (300 μM) for 60 min (Fig. 2D, right trace) or to the PKA/PKG inhibitor H89 (50 μM) for 60 min (Fig. 2E, right trace). PKA activation increased the KCNQ1/KCNE1 current in a time-dependent manner and 60 min of activation increased the current obtained at 20 mV to 149.5 $\pm$ 21.5% of control, $n = 5$ (Fig. 2F). Inhibition of PKA by H89 reduced the current obtained at 20 mV to 74.4 $\pm$ 6.1%, $n = 3$, which suggests a basal level of PKA activity. Thus, PKG and PKA inhibition and activation by membrane-permeable inhibitors and cGMP- or cAMP analogs is robust and efficient in *Xenopus laevis* oocytes.

A mutational strategy was adopted to further deduce a possible involvement of Ser^{111} in a gating mechanism of AQP4. Ser^{111} was mutated to an alanine (S111A) to abolish potential phosphorylation of this residue and to an aspartate (S111D) in an attempt to mimic a phosphorylated serine (Maciejewski et al., 1995). The wild type AQP4 and the two mutant constructs, AQP4.S111A and AQP4.S111D, were expressed in oocytes and the water permeability was determined. The water permeabilities of these constructs in a representative batch of oocytes ($n = 5$ of each construct) are shown in Fig. 3A with water permeabilities of (in $\times 10^{-3}$ cm/s): 1.67 $\pm$ 0.18 for wild-type AQP4, 1.47 $\pm$ 0.10 for AQP4.S111A, and 1.20 $\pm$ 0.20 for AQP4.S111D, $n = 5$. As membrane expression levels vary between batches of oocytes and between constructs, we semiquantified the membrane abundance of oocytes from each day-matched batch of oocytes ($n = 5$ of each construct) by immunocytochemistry. Representative confocal images are shown in Fig. 3B and the membrane abundance of the different constructs in the representative batch from Fig. 3A is summarized in Fig. 3C. AQP4.S111A and AQP4.S111D both act as functional water channels at the plasma membrane. Based on the water permeability and the membrane abundance of each individual construct, the relative unit water permeability was obtained for each batch of oocytes. The relative unit water permeability was normalized to that of the wild-type AQP4 and averaged across four to five experimental batches of oocytes (Fig. 3D). There was no significant difference between the relative unit water permeability of AQP4 and the two mutants AQP4.S111A and AQP4.S111D (in % of AQP4 WT): 109 $\pm$ 10.5% for AQP4.S111A, $n = 5$ and 117 $\pm$ 9.4% for AQP4.S111D, $n = 4$. Therefore a phosphorylated Ser^{111} is not required for AQP4 to be fully functional and an attempt to mimic a phosphorylation at Ser^{111} does not significantly increase the water permeability of AQP4.

Astrocytic Water Permeability

AQP4 is native to the astrocytes of the mammalian central nervous system where it is highly expressed in the perivascular

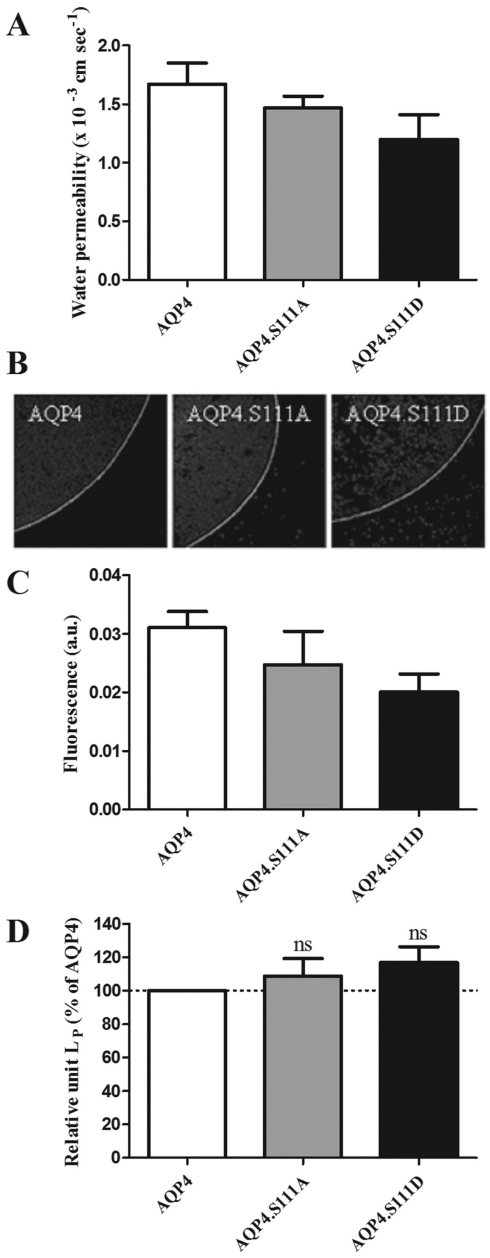

FIGURE 3: No change in the relative unit water permeability by mutation of Ser^{111}. (A) A representative experiment of the average water permeability of oocytes expressing AQP4, AQP4.S111A, or AQP4.S111D obtained as in Fig. 1 ($n = 5$). The contribution from the native oocyte membrane was deducted prior to quantification of the AQP4-mediated water permeability. (B) Representative confocal laser scanning microscopy of oocytes expressing either AQP4 (left panel), AQP4.S111A (middle panel), or AQP4.S111D (right panel) after immunolabeling with anti-AQP4 antibodies. (C) Oocyte plasma membrane fluorescent counts of oocytes from the same experiment as in panel A, were used to assess the AQP4 abundance in the plasma membrane of AQP4-, AQP4.S111A-, and AQP4.S111D-expressing oocytes ($n = 5$). (D) Relative unit water permeability (values obtained as in panel A divided by values obtained as in C) of AQP4.S111A and AQP4.S111D was normalized to that of AQP4 and averaged across 4-5 experiments. In % of control; 109 $\pm$ 10.5 for AQP4.S111A, $n = 5$ and 117 $\pm$ 9.4 for AQP4.S111D, $n = 4$. ANOVA followed by Dunnett's multiple comparison test was used as statistical test.

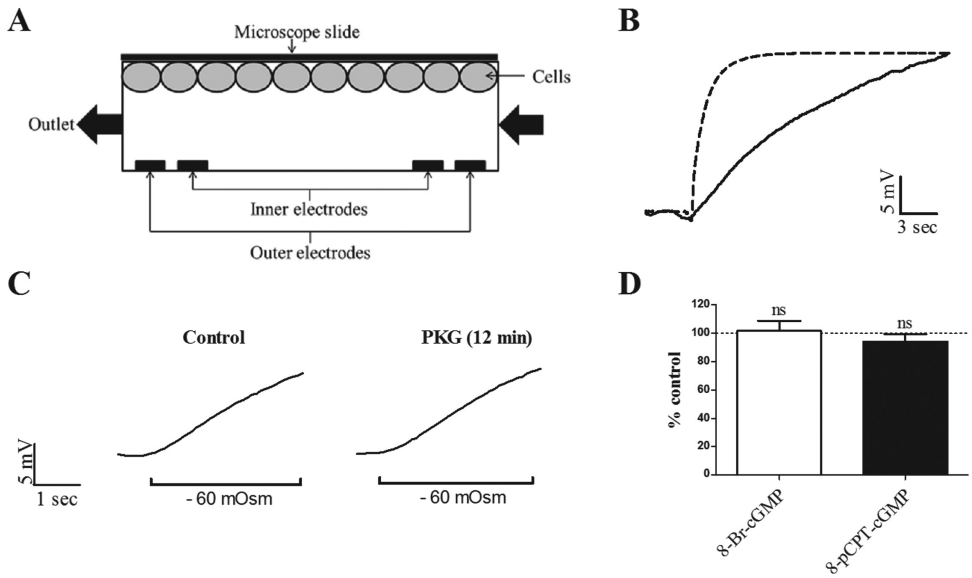

FIGURE 4: Astrocytic water permeability was not affected by PKG activation. (A) Schematic representation of the microfluidic volume sensor with the sensing chamber, electrodes, and cell-containing slide. (B) The speed of solution change (dashed line) precedes the osmotically induced change in astrocytic cell volume (solid line). (C) Representative traces from astrocytes in primary culture challenged with a hyposmotic gradient prior to (left panel) and after (right panel) exposure of a PKG-activator (8-Br-cGMP, 100 μM). Measurements were performed in duplicates prior to and after addition of either 8-pCPT-cGMP or 8-Br-cGMP (both 100 μM). (D) Summarized astrocytic water permeabilities after stimulation with the PKG activators normalized to the control measurements, n = 5–6 based on three batches of astrocyte culture for each cGMP-analog. In % of control; 101.7 ± 7.1 for 8-Br-cGMP, n = 5 and 93.9 ± 5.4 for 8-pCPT-cGMP, n = 6. Paired Student's t-test was used as statistical test.

endfeet (Nielsen et al., 1997). In primary culture of astrocytes, AQP4 loses its distinct expression pattern and disperses throughout the entire plasma membrane (Nicchia et al., 2000). The entire astrocytic surface is thus provided with an AQP4-dependent osmotic water permeability. We used primary cultures of astrocytes to determine the effect of PKG activation on AQP4. We employed a microfluidic cell volume sensor (Ateya et al., 2005), which meets the required experimental criteria of swift solution change and fast sampling rate, to measure the osmotic water permeability of the astrocytic culture (Fig. 4A). The premise is based on placing the cells in a small sensing chamber and applying a constant current through the chamber. Upon cell swelling, the free volume of the sensing chamber is reduced and the electric resistance therefore increased. The change in voltage is thus a sensitive and robust read-out of cell volume changes and is stable over the entire duration of the experiment. Upon a swift solution change to a test solution containing 60 mOsm less mannitol than the control solution, the astrocytes swelled immediately as illustrated by the solid trace in Fig. 4B. The dotted line indicates the rate of solute change which clearly precedes the rate of cell swelling. The astrocytes were exposed to two consecutive hyposmotic challenges, a representative trace of which is shown in Fig. 4C, left trace. Subsequently, the astrocytes were exposed to the membrane-permeable cGMP analog (8-Br-cGMP, 100 μM, 12 min) before exposure to hyposmotic challenges identical to those of the control except the presence of 8-Br-cGMP in both control and hyposmotic test solution (Fig. 4C, right trace). PKG has repeatedly been shown to be activated in cultured astrocytes by membrane-permeable analogs of cGMP (Brahmachari et al., 2006; Konopacka et al., 2009; Sporbert et al., 1999). The rate of osmotically-induced astrocytic swelling was identical before and after exposure to the PKG activator. The data, along with those obtained with the alternative PKG activator, 8-pCPT-cGMP, are summarized in Fig. 4D where the rate of astrocytic cell swelling upon exposure to cGMP analogs is presented as % of that of the control; 101.7 ± 7.1, n = 5 for 8-Br-cGMP and 93.9 ± 5.4, n = 6 for 8-pCPT-cGMP.

Molecular Dynamics Simulations

Molecular dynamics simulations were performed on AQP4 to obtain a scenario in which a phosphate-group was attached to Ser^{111} (Fig. 5A). In the simulation time window, we observed no significant effect of the phosphorylation of Ser^{111} (pS111-AQP4) on the conformation of the Ser^{111}-containing loop B or of the loop D (Fig. 5B). Nor did the phosphorylation of Ser^{111} affect the water permeability of AQP4, (in $\times 10^{-14}$ cm^3/sec); 1.93 ± 0.41 for AQP4 and 1.94 ± 0.39 for pS111-AQP4, n = 8 (Fig. 5C). To determine the effect of a phosphorylation of Ser^{111} on the flexibility of the B-loop, we compared the Root Mean Square Fluctuations (RMSF) of the

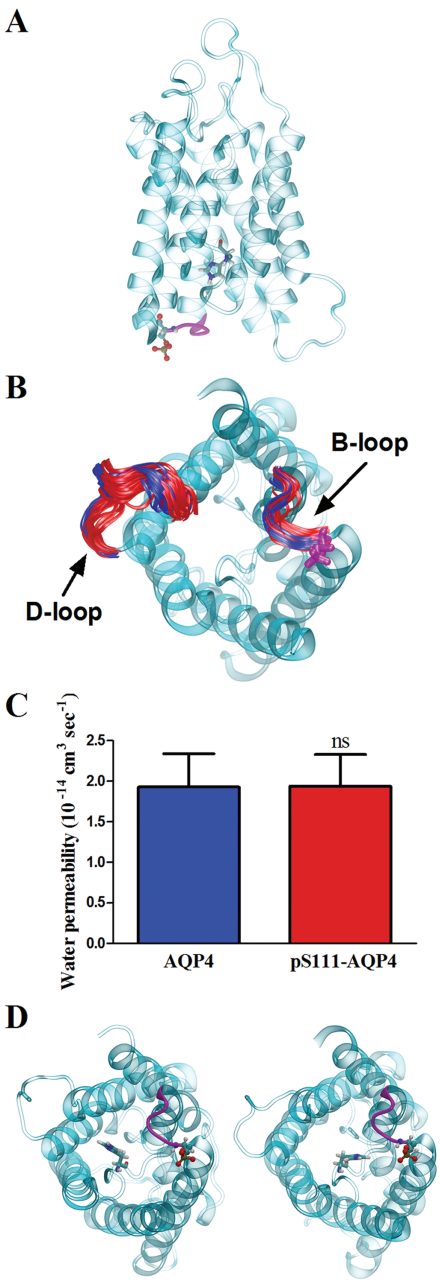

FIGURE 5: Molecular dynamics simulation on AQP4 revealed no functional effect of phosphorylation of Ser^{111} on the water permeability of AQP4. (A) Side-view of an AQP4 monomer with the B loop in magenta and with a phosphate-group (shown in ball and stick model) attached to Ser^{111}. His^{95} is emphasized in licorice representation. (B) Recorded conformations of the B and D loop in the non-phosphorylated (blue) and the phosphorylated form (red), viewed from the intracellular side. The average position of phosphorylated Ser^{111} is shown in licorice representation. The phosphorylated and non-phosphorylated conformations largely overlap and neither blocked the channel. (C) The summarized recorded water permeability of AQP4 whether non-phosphorylated (blue) or phosphorylated (red) was not statistically different (n = 8 blocks, Student's t-test). (D) View of an AQP4 monomer from the intracellular side with loop B in magenta and the phosphorylated Ser^{111} depicted in ball and stick representation. His^{95}, shown in licorice representation, transiently moves into (left panel) and out of (right panel) the pore during the simulation.

backbone atoms of the loop residues over 400 ns of the simulation. There was no significant change in the motion of the loop between the phosphorylated and the non-phosphorylated forms (data not shown). During the simulation, His^{95} was discovered to transiently move in and out of the channel pore of the AQP4 (Fig. 5D). In the initial simulations, we had predicted this residue to have a single protonation and thus be neutral. Since this residue was placed within 1 nm distance of the Ser^{111}, a protonation of this His^{95} could possibly prevent it from blocking the channel pore by electrostatic interaction with the negatively charged phosphate-moiety attached to Ser^{111}. His^{95} might thus become doubly protonated, due to a pK_a shift upon phosphorylation, and thereby change its conformation and transiently block the water pore. To test this hypothesis, we used both the doubly protonated and the neutral (singly protonated at epsilon nitrogen) forms of this histidine in simulations. However, also in the simulations with a doubly protonated His^{95} did we observe no significant difference in the water permeability between the two forms of AQP4 (data not shown).

No Detectable In Vivo *Phosphorylation of Ser^{111}*

Phosphorylation of Ser^{111} is the proposed molecular determinant for the putative gating mechanism for AQP4. A PKG-dependent phosphorylation of a *peptide* encoding the respective consensus sequence has been demonstrated (Gunnarson et al., 2008) but *in vivo* or *in vitro* phosphorylation of whole-length AQP4 at this residue has not. We generated a phospho-specific antibody that recognizes an epitope surrounding the Ser^{111} *solely* when the Ser^{111} is phosphorylated, pS111-AQP4 (Fig. 6A). The selectivity toward the phosphorylated peptide is demonstrated by dot blot with the native and the phosphorylated peptides encoding the region in question, i.e., the antibody epitope (Fig. 6B).

Rat brain slices were incubated 60 min in the presence or absence of the mGluR agonist DHPG, which has been proposed to induce downstream PKG-dependent phosphorylation of AQP4 at Ser^{111} (Gunnarson et al., 2008). Brain homogenate was subsequently prepared in the presence of a cocktail of phosphatase inhibitors to preserve possible phosphorylation of AQP4. Immunoblots of the brain homogenate were performed with either the conventional C-terminal AQP4 antibody (Fig. 6C, left panel) or the pS111-AQP4 antibody (Fig 6C, right panel). The left lane in both panels is loaded with the brain homogenate of slices kept in control solution and the right lane in both panels is loaded with the homogenate of slices exposed to DHPG. The three different isoforms of AQP4, M1, M23, and Mz (Moe et al., 2008), were visible on the immunoblot based on the conventional AQP4 antibody (Fig. 6C, left panel) whereas no immunoreactivity was detected with the pS111-AQP4 antibody

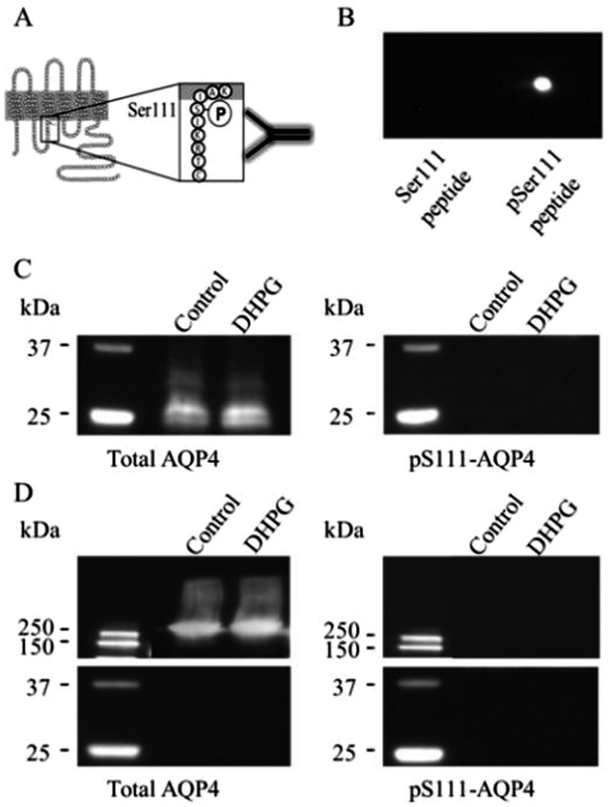

FIGURE 6: No evidence in favor of *in vivo* phosphorylation of Ser^{111} on AQP4 in rat brain. (A) A schematic diagram depicting the epitope recognized by the phospho-specific antibody pS111-AQP4. (B) Dot blot analysis demonstrates that the anti-pS111-AQP4 antibody recognizes exclusively the AQP4 peptide encoding the *phosphorylated* Ser^{111} and not the peptide encoding the non-phosphorylated Ser^{111}. (C, D) Immunoblotting of whole rat brain lysate incubated 60 min in either a control solution (lane 1) or a solution containing 50 μM of the mGluR1/5 agonist DHPG (lane 2); left panel with a conventional C-terminal anti-AQP4 antibody and right panel with the custom-made pS111-AQP4 antibody (size marker on left side of all blots). Before loading, samples were (C) kept at room temperature or (D) heated to 90°C. The total amount of AQP4 was unaffected by treatment with DHPG (left panels) and no immuno-reactivity was detected with the pS111-AQP4 antibody regardless of DHPG treatment (right panels), $n = 3$.

(Fig. 6C, right panel), $n = 3$. As steric hindrance of the antibody to its epitope cannot be ruled out, we attempted to alter the accessibility of the epitope by complete denaturation of AQP4: a separate sample of the brain homogenate was heated to 90°C before immunoblotting. This treatment, in association with the denaturing process, promotes aggregation of AQP4 (Sorbo et al., 2007), which is thus detected at higher molecular weight when immunoblotted with the conventional antibody (Fig. 6D, left panel). No immuno-reactivity of the pS111-AQP4 antibody was observed under these conditions (Fig. 6D, right panel). Exposure of the brain slice to DHPG did not induce detectable phosphorylation of AQP4 on Ser^{111}, indicating that AQP4 may not be phosphorylated in this manner *in vivo*.

Discussion

In the present work we have addressed the controversial issue of phosphorylation-dependent gating of AQP4 as a physiological mechanism for regulation of the osmotic water permeability of AQP4-expressing astrocytes. The low intrinsic osmotic water permeability of the plasma membrane of *Xenopus laevis* oocytes makes this heterologous expression system ideal for quantitative studies of water permeability of select proteins. The water permeability of *Xenopus* oocytes increased ~15-fold following expression of AQP4, in line with previous reports (e.g., Fenton et al., 2010). The AQP4-mediated water permeability was not increased by PKG or PKA activation, nor was it reduced by inhibition of these protein kinases. These experiments were performed with each oocyte as its own control, thus solidifying the obtained data by exclusion of individual expression levels as a factor of variance. The sensitivity of the experimental system toward protein kinase-mediated changes in water permeability has previously been documented: PKC-activation reduced the water permeability of AQP4-expressing oocytes (Fenton et al., 2010; Moeller et al., 2009a) in line with observations in an AQP4-expressing mammalian cell line (Zelenina et al., 2002). We verified the presence of both cGMP-activated PKG and cAMP-activated PKA in *Xenopus* oocytes; evident as a robust PKG-induced activation of the epithelial Na^+-channel, ENaC (Nie et al., 2009) or as a PKA-induced activation of the voltage-gated K^+-channel KCNQ1/KCNE1 (Dilly et al., 2004; Grunnet et al., 2003). Site-directed mutagenesis of Ser^{111} to an alanine prevents a putative phosphorylation of this residue. Nevertheless, this mutated form of AQP4 (S111A) displayed unit water permeability identical to that of the wild type AQP4. Similarly, mimicking a Ser^{111} phosphorylation by introducing an aspartic acid residue in place of Ser^{111} did not increase the AQP4-mediated water permeability.

AQP4 is highly expressed in astrocytes of the mammalian central nervous system (Nielsen et al., 1997) and is a major contributor to the osmotic water permeability of the astrocyte plasma membrane (Solenov et al., 2004). To determine the PKG-dependent regulatory impact on AQP4 in a more native setting, we measured the effect of PKG activation on the osmotic water permeability of astrocytes in primary culture. To study water permeability in small, highly water permeable cells with a large surface to volume ratio, a fast sampling rate is of absolute necessity to obtain the initial linear cell swelling. This initial segment represents the osmotic water permeability of the astrocytic membrane. Our data show that the solution exchange rate in the microfluidic volume sensor exceeds that of the cell swelling and thus ensures that the rate-limiting step for the cell volume response is the water permeability of the cell and not that of the solution change (Heo et al., 2008; Solenov et al., 2004). We obtained

no evidence for a PKG-dependent effect on the water permeability of the AQP4-containing astrocytic membrane.

Taken together, our data demonstrate a complete absence of Ser^{111} phosphorylation-dependent increase in AQP4-mediated water permeability. This conclusion is in contrast to earlier reports of kinase-dependent gating of AQP4 (Gunnarson et al., 2005, 2008; Song and Gunnarson 2012). In these studies CaMKII, PKA, and PKG were all, based on similar approaches, proposed to lead to phosphorylation of AQP4 on Ser^{111} and thereby increase AQP4-mediated water permeability. Activation of the metabotropic glutamate receptors mGluR1/5 in the astrocytic membrane was suggested to induce a signaling cascade of Ca^{2+} release, activation of CaMKII and subsequent induction of NO-synthase and associated NO production. NO would in turn induce cGMP generation followed by PKG-dependent increase of AQP4-mediated water permeability (Gunnarson et al., 2008). No PKG-dependent increase in water permeability was observed upon expression of AQP4 with the Ser^{111} mutated to an alanine (Gunnarson et al., 2008). Based thereupon, phosphorylation of this residue was claimed as the regulatory switch. Although the reason for the contradictory data is not clear, a few technical issues may offer at least a partial explanation: (i) The data in Gunnarson et al. (2005, 2008), and Song and Gunnarson (2012) were obtained with a sample rate of one scan every 2 s, i.e., 0.5 Hz (data in present study obtained with continuous recording), (ii) the water permeability was calculated from the values obtained within the first 6–10 seconds after introduction of the osmotic challenge (we use the values obtained within the initial couple of seconds, where the cell swelling is linear and maximal and therefore represents the osmotic water permeability of the cell membrane), (iii) the authors performed their experiments at 10°C in Gunnarson et al. (2005), and (iv) did not provide verification that the speed of solution change exceeded that of the rate of volume change. Since the same cells never acted as their own control, one cannot rule out that minor unaccounted-for differences in cell size between cells transfected with different constructs or the native cells used for background-subtraction (as previously observed (Silberstein et al., 2004)) could have affected their calculated osmotic water permeabilities.

Ser^{111} is conserved in human, mouse and rat AQP4 and corresponds to Ser^{115} in the spinach aquaporin SoPIP2;1 (Gunnarson et al., 2008). The crystal structure of SoPIP2;1 was determined in an open and a closed confirmation and molecular dynamics simulations were performed on the basis of this crystal structure (Tornroth-Horsefield et al., 2006). The simulations recorded an open conformation of the water channel when a phosphate-moiety, *in silico*, was attached to Ser^{115}. The authors predicted this to be due to an interaction between the D-loop and the N-terminus which would anchor the loop onto the cytoplasmic entrance to the pore (Tornroth-Horsefield et al., 2006). The 1.8Å crystal structure of AQP4 was recently obtained in an *open* conformation despite no indication of the presence of a phosphate-moiety on Ser^{111} (Ho et al., 2009). The D-loop of the AQP4 was, in addition, deemed too short to serve the role of a gate (Ho et al., 2009) which thus argues against phosphorylation-dependent gating of AQP4 with Ser^{111} as the molecular switch.

In our molecular dynamics simulations on AQP4, we did not observe a significant difference between the water permeability of AQP4 and its phosphorylated form. The motion of the B-loop that contains the Ser^{111} and of the D-loop was restricted in either form, in line with the observation that the D-loop may be too short for a large structural change (Ho et al., 2009). The protonation of His^{95}, positioned above the channel pore opposite loop B, might be affected by the phosphorylation state of the Ser^{111}. To probe for this possibility, simulations of a doubly protonated His^{95} were carried out. However, no interaction between His^{95} and the phosphorylated serine was observed in the simulations. Accordingly, no significant difference in the calculated water permeability between the two forms of AQP4 was observed, leading us to infer that electrostatic interaction between the histidine (His^{95}) and the phosphorylated serine (Ser^{111}) did not affect the channel gating. Thus the simulations carried out in the present study do not indicate any effect of phosphorylation of Ser^{111} on movement of loops B and D and thus gating of AQP4.

Lack of phosphorylation-dependent changes of the water permeability of AQP4 could be caused by the absence of a functional outcome of a given phosphorylation or a complete lack of phosphorylation of the residue in question. It has been demonstrated that PKG and PKA are indeed able to phosphorylate Ser^{111}, *in vitro,* on a peptide corresponding to the sequence around Ser^{111} but determination of the phosphorylated state of this residue in the intact protein was not attempted (Gunnarson et al., 2008; Song and Gunnarson, 2012). To assess the latter possibility, we generated a custom-made phospho-specific antibody designed to recognize the epitope containing Ser^{111} only when this residue is phosphorylated. The antibody recognized a phosphorylated peptide containing the Ser^{111} while showing no immune-reactivity toward the non-phosphorylated peptide. We did not detect Ser^{111}-phosphorylated AQP4 in rat brain treated with an mGluR1/5 analog proposed to induce phosphorylation of this very residue (Gunnarson et al., 2008). We lack, however, a good positive control at the whole-protein level, and therefore cannot completely exclude that steric hindrance might block the epitope from antibody binding in the intact protein. With the phospho-specific antibody, we performed immunoblot on semi- and completely denatured AQP4 as well as immunohistochemistry on rat and mouse kidney slices that express high levels of AQP4 in specific cell types (data not

shown). From these experimental paradigms, one may expect three different levels of epitope accessibility, neither of which yielded a positive immune-response with this antibody. Taken together with the elaborate, yet unsuccessful, experimental effort to induce *in vivo* phosphorylation of Ser^{115} in SoPIP2;1 (Johansson et al., 1998), our data suggest that Ser^{111} remains unphosphorylated *in vivo*. Unfortunately, attempts to validate these data by means of mass spectrometry were unsuccessful, as the particular peptide fragment containing the Ser^{111} residue was not amenable to detection by mass spectrometry.

AQP4, as well as phosphorylation-dependent regulation thereof, has been suggested to be a possible mediator of K^+- and glutamate-induced cell swelling as well as cytotoxic brain edema formation. Curiously, experimental evidence to that effect is generally obtained upon addition of large, non-physiologically occurring osmotic gradients in the order of 100-200 mOsm (Gunnarson et al., 2005, 2008; Nicchia et al., 2000; Solenov et al., 2004; Song and Gunnarson, 2012). The calculated osmotic water permeabilities have then been inferred to represent physiologically applicable water transport. It should be noted that such osmotic gradients across the astrocytic membrane are unlikely to arise; the highly water-permeable astrocytes will remain in osmotic equilibrium with their surroundings upon small perturbations of transmembranous osmotic gradients well within a sub-second timescale. Note the rapidly-achieved equilibrium observed in astrocytes (both with and without AQP4 expression) upon challenge with a large osmotic gradient at 37°C (Solenov et al., 2004). Accordingly, the rate-limiting factor for astrocytic cell swelling will be either osmolyte accumulation or activity of water-translocating cotransporters (for review see MacAulay and Zeuthen (2010, 2012)). In fact, it was recently demonstrated that AQP4-deficient mice display *increased* stimulus-induced astrocytic cell swelling compared to their WT counterpart (Haj-Yasein et al., 2012), thus providing evidence against AQP4 as a mediator of astrocytic cell swelling during neuronal activity.

In conclusion, we detect no evidence in favor of phosphorylation-dependent gating of AQP4 via Ser^{111}, whether in cultured astrocytes or upon heterologous expression of AQP4 in oocytes (with or without an intact Ser^{111}). AQP4 phosphorylated at Ser^{111} was not detected *in vivo* and experimental mimicking of a phosphorylated Ser^{111}, whether with a mutational strategy or via molecular dynamics simulations, recorded no difference in the water permeability of AQP4. Thus, phosphorylation-dependent gating of AQP4 at Ser^{111} is not, as earlier proposed, the molecular switch for astrocytic cell swelling or brain edema formation.

Acknowledgment

Grant sponsors: Lundbeck Foundation (to N.M., M.A., and R.A.F.), Danish Medical Research Council (to N.M. and R.A.F.), Novo Nordisk Foundation (to N.M. and R.A.F.), National Institutes of Health; Grant number: DK\-77302 (to S.Z.H.); Grant sponsor: Max Planck Society (to S.K. and B.dG.).

The authors greatly value the technical assistance provided by Charlotte Goos Iversen, Catia Correa Goncalves Andersen, Mary Teeling, Inger-Merete Paulsen, and Bodil Kruse. The authors' gratitude goes to the inventors of the microfluidic volume sensor: Drs. Susan Z. Hua, Fred Sachs, and Steve Besch at University of Buffalo. The authors highly appreciate Dr. Hua's generosity of including Mette Assentoft into her laboratory to conduct the present experiments and the technical advice provided by Jason Rahimzadeh. The authors are grateful to Michael Lund Nielsen at the Copenhagen Protein Center for his willingness to perform the mass spectrometry and to Kamilla Angelo for technical assistance with the rat brain preparation. The authors thank Dr. Camilo Aponte Santamaria for the implementation of the collective diffusion constant measurement for Gromacs.

References

Ateya DA, Sachs F, Gottlieb PA, Besch S, Hua SZ. Volume cytometry: Microfluidic sensor for high-throughput screening in real time. Anal Chem 2005;77:1290–1294.

Berendsen HJC, Grigera JR, Straatsma TP. The missing term in effective pair potentials. J Phys Chem 1987;91:6269–6271.

Berger O, Edholm O, Jahnig F. Molecular dynamics simulations of a fluid bilayer of dipalmitoylphosphatidylcholine at full hydration, constant pressure, and constant temperature. Biophys J 1997;72:2002–2013.

Brahmachari S, Fung YK, Pahan K. Induction of glial fibrillary acidic protein expression in astrocytes by nitric oxide. J Neurosci 2006;26:4930–4939.

Bussi G, Donadio D, Parrinello M. Canonical sampling through velocity rescaling. J Chem Phys 2007;126:014101.

Darden T, York D, Pedersen L. Particle mesh Ewald—An N.Log(N) method for Ewald sums in large systems. J Chem Phys 1993;98:10089–10092.

Dilly KW, Kurokawa J, Terrenoire C, Reiken S, Lederer WJ, Marks AR, Kass RS. Overexpression of beta2-adrenergic receptors cAMP-dependent protein kinase phosphorylates and modulates slow delayed rectifier potassium channels expressed in murine heart: evidence for receptor/channel co-localization. J Biol Chem 2004;279:40778–40787.

Feenstra KA, Hess B, Berendsen HJC. Improving efficiency of large time-scale molecular dynamics simulations of hydrogen-rich systems. J Comput Chem 1999;20:786–798.

Fenton RA, Moeller HB, Zelenina M, Snaebjornsson MT, Holen T, MacAulay N. Differential water permeability and regulation of three aquaporin 4 isoforms. Cell Mol Life Sci 2010;67:829–840.

Friedman B, Schachtrup C, Tsai PS, Shih AY, Akassoglou K, Kleinfeld D, Lyden PD. Acute vascular disruption and aquaporin 4 loss after stroke. Stroke 2009;40:2182–2190.

Frydenlund DS, Bhardwaj A, Otsuka T, Mylonakou MN, Yasumura T, Davidson KG, Zeynalov E, Skare O, Laake P, Haug FM, Rash JE, Agre P, Ottersen OP, Amiry-Moghaddam M. Temporary loss of perivascular aquaporin-4 in neocortex after transient middle cerebral artery occlusion in mice. Proc Natl Acad Sci USA 2006;103:13532–13536.

Grunnet M, Jespersen T, MacAulay N, Jorgensen NK, Schmitt N, Pongs O, Olesen SP, Klaerke DA. KCNQ1 channels sense small changes in cell volume. J Physiol 2003;549:419–27.

Gunnarson E, Axehult G, Baturina G, Zelenin S, Zelenina M, Aperia A. Lead induces increased water permeability in astrocytes expressing aquaporin 4. Neuroscience 2005;136:105–114.

Gunnarson E, Zelenina M, Axehult G, Song Y, Bondar A, Krieger P, Brismar H, Zelenin S, Aperia A. Identification of a molecular target for glutamate regulation of astrocyte water permeability. Glia 2008;56:587–596.

Haj-Yasein NN, Jensen V, Ostby I, Omholt SW, Voipio J, Kaila K, Ottersen OP, Hvalby O, Nagelhus EA. Aquaporin-4 regulates extracellular space volume dynamics during high-frequency synaptic stimulation: A gene deletion study in mouse hippocampus. Glia 2012;60:867–874.

Heo J, Meng F, Hua SZ. Contribution of aquaporins to cellular water transport observed by a microfluidic cell volume sensor. Anal Chem 2008;80: 6974–6980.

Hess B. P-LINCS: A parallel linear constraint solver for molecular simulation. J Chem Theory Comput 2008;4:116–122.

Hess B, Kutzner C, van der Spoel D, Lindahl E. GROMACS 4: Algorithms for highly efficient, load-balanced, and scalable molecular simulation. J Chem Theory Comput 2008;4:435–447.

Ho JD, Yeh R, Sandstrom A, Chorny I, Harries WE, Robbins RA, Miercke LJ, Stroud RM. Crystal structure of human aquaporin 4 at 1.8 A and its mechanism of conductance. Proc Natl Acad Sci USA 2009;106:7437–7442.

Homeyer N, Horn AHC, Lanig H, Sticht H. AMBER force-field parameters for phosphorylated amino acids in different protonation states: Phosphoserine, phosphothreonine, phosphotyrosine, and phosphohistidine. J Mol Model 2006;12:281–289.

Johansson I, Karlsson M, Shukla VK, Chrispeels MJ, Larsson C, Kjellbom P. Water transport activity of the plasma membrane aquaporin PM28A is regulated by phosphorylation. Plant Cell 1998;10:451–459.

Konopacka A, Konopacki FA, Albrecht J. Protein kinase G is involved in ammonia-induced swelling of astrocytes. J Neurochem 2009;109:246–251.

Langan TJ, Plunkett RJ, Asada H, Kelly K, Kaseloo P. Long-term production of neurotrophic factors by astrocyte cultures from hemiparkinsonian rat brain. Glia 1995;14:174–184.

Lindorff-Larsen K, Piana S, Palmo K, Maragakis P, Klepeis JL, Dror RO, Shaw DE. Improved side-chain torsion potentials for the Amber ff99SB protein force field. Proteins 2010;78:1950–1958.

MacAulay N, Zeuthen T. Water transport between cns compartments: Contributions of aquaporins and cotransporters. Neuroscience 2010;168: 941–956.

MacAulay N, Zeuthen T. Glial K(+) clearance and cell swelling: Key roles for cotransporters and pumps. Neurochem Res 2012;37:2299–309.

Maciejewski PM, Peterson FC, Anderson PJ, Brooks CL. Mutation of serine-90 to glutamic-acid mimics phosphorylation of bovine prolactin. J Biol Chem 1995;270:27661–27665.

Meng S, Qiao M, Lin L, Del Bigio MR, Tomanek B, Tuor UI. Correspondence of AQP4 expression and hypoxic-ischaemic brain oedema monitored by magnetic resonance imaging in the immature and juvenile rat. Eur J Neurosci 2004;19:2261–2269.

Moe SE, Sorbo JG, Sogaard R, Zeuthen T, Ottersen P, Holen T. New isoforms of rat Aquaporin-4. Genomics 2008;91:367–377.

Moeller HB, Fenton RA, Zeuthen T, Macaulay N. Vasopressin-dependent short-term regulation of aquaporin 4 expressed in Xenopus oocytes. Neuroscience 2009a;164:1674–1684.

Moeller HB, MacAulay N, Knepper MA, Fenton RA. Role of multiple phosphorylation sites in the COOH-terminal tail of aquaporin-2 for water transport: Evidence against channel gating. Am J Physiol Renal Physiol 2009b;296:F649–F657.

Nicchia GP, Frigeri A, Liuzzi GM, Santacroce MP, Nico B, Procino G, Quondamatteo F, Herken R, Roncali L, Svelto M. Aquaporin-4-containing astrocytes sustain a temperature- and mercury-insensitive swelling in vitro. Glia 2000;31:29–38.

Nie HG, Chen L, Han DY, Li J, Song WF, Wei SP, Fang XH, Gu X, Matalon S, Ji HL. Regulation of epithelial sodium channels by cGMP/PKGII. J Physiol 2009;587:2663–2676.

Nielsen S, Nagelhus EA, Amiry-Moghaddam M, Bourque C, Agre P, Ottersen OP. Specialized membrane domains for water transport in glial cells: High-resolution immunogold cytochemistry of aquaporin-4 in rat brain. J Neurosci 1997;17:171–180.

Papadopoulos MC, Verkman AS. Aquaporin-4 gene disruption in mice reduces brain swelling and mortality in pneumococcal meningitis. J Biol Chem 2005;280:13906–13912.

Ribeiro Mde C, Hirt L, Bogousslavsky J, Regli L, Badaut J. Time course of aquaporin expression after transient focal cerebral ischemia in mice. J Neurosci Res 2006;83:1231–1240.

Rusinova R, Shen YM, Dolios G, Padovan J, Yang H, Kirchberger M, Wang R, Logothetis DE. Mass spectrometric analysis reveals a functionally important PKA phosphorylation site in a Kir3 channel subunit. Pflugers Arch 2009;458: 303–314.

Saadoun S, Papadopoulos MC, Krishna S. Water transport becomes uncoupled from K+ siphoning in brain contusion, bacterial meningitis, and brain tumours: immunohistochemical case review. J Clin Pathol 2003;56: 972–975.

Silberstein C, Bouley R, Huang Y, Fang P, Pastor-Soler N, Brown D, Van Hoek AN. Membrane organization and function of M1 and M23 isoforms of aquaporin-4 in epithelial cells. Am J Physiol Renal Physiol 2004;287: F501–F511.

Solenov E, Watanabe H, Manley GT, Verkman AS. Sevenfold-reduced osmotic water permeability in primary astrocyte cultures from AQP-4-deficient mice, measured by a fluorescence quenching method. Am J Physiol Cell Physiol 2004;286:C426–C432.

Song Y, Gunnarson E. Potassium dependent regulation of astrocyte water permeability is mediated by cAMP signaling. PloS One 2012;7:e34936.

Sorbo JG, Moe SE, Holen T. Early upregulation in nasal epithelium and strong expression in olfactory bulb glomeruli suggest a role for Aquaporin-4 in olfaction. FEBS Lett 2007;581:4884–4890.

Sporbert A, Mertsch K, Smolenski A, Haseloff RF, Schonfelder G, Paul M, Ruth P, Walter U, Blasig IE. Phosphorylation of vasodilator-stimulated phosphoprotein: a consequence of nitric oxide- and cGMP-mediated signal transduction in brain capillary endothelial cells and astrocytes. Brain Res Mol Brain Res 1999;67:258–266.

Tornroth-Horsefield S, Wang Y, Hedfalk K, Johanson U, Karlsson M, Tajkhorshid E, Neutze R, Kjellbom P. Structural mechanism of plant aquaporin gating. Nature 2006;439:688–694.

Walz T, Fujiyoshi Y, Engel A. The AQP structure and functional implications. Handb Exp Pharmacol 2009;190:31–56.

Wolf MG, Hoefling M, Aponte-Santamaria C, Grubmuller H, Groenhof G. g_membed: Efficient insertion of a membrane protein into an equilibrated lipid bilayer with minimal perturbation. J Comput Chem 2010;31:2169–2174.

Zador Z, Stiver S, Wang V, Manley GT. Role of aquaporin-4 in cerebral edema and stroke. Handb Exp Pharmacol 2009;190:159–170.

Zelenina M, Zelenin S, Bondar AA, Brismar H, Aperia A. Water permeability of aquaporin-4 is decreased by protein kinase C and dopamine. Am J Physiol Renal Physiol 2002;283:F309–F318.

Zeuthen T, Belhage B, Zeuthen E. Water transport by Na+-coupled cotransporters of glucose (SGLT1) and of iodide (NIS). The dependence of substrate size studied at high resolution. J Physiol 2006;570:485–499.

Zhao J, Moore AN, Clifton GL, Dash PK. Sulforaphane enhances aquaporin-4 expression and decreases cerebral edema following traumatic brain injury. J Neurosci Res 2005;82:499–506.

Zhu FQ, Tajkhorshid E, Schulten K. Collective diffusion model for water permeation through microscopic channels. Phys Rev Lett 2004;93:224501.